Preliminary Assessment of the Importance of Platform–Tendon Coupling in a Tension Leg Platform

Marco Masciola and Meyer Nahon
Department of Mechanical Engineering
McGill University
Montreal, Quebec, H3A 2K6
Canada

Frederick Driscoll
National Renewable Energy Laboratory
Golden, CO, 80401
USA

May 2012

Abstract

This paper presents performance metrics that can be used to evaluate the response sensitivity of a Tension Leg Platform (TLP) to its tendons. An uncoupled TLP model ignores the intrinsic dynamics and environmental loads on the cables by treating each tendon as an ideal massless spring. A coupled TLP system, in contrast, considers the effects of distributed mass and drag along the tendon. Under certain operating conditions, an uncoupled dynamics model can produce results comparable to its coupled counterpart. This paper defines the conditions under which it is acceptable to model a TLP tendon as a linear spring, as opposed to one that considers the cable dynamics. The analysis is performed in the frequency domain and, for generality, the results are non–dimensionalized. The findings indicate that a more elaborate set of conditions than the platform–to–cable mass ratio must be satisfied for the two models to provide similar results. To conclude this study, two simulations are performed and compared against the performance metrics derived in this paper.

1 Introduction

A Tension Leg Platform (TLP) can be described as an offshore structure consisting of a buoyant body tethered to the sea floor by a series of pretensioned cables. A TLP is generally viewed as an assembly with two main components: the surface vessel and the tendons. Each component imparts its own unique dynamic characteristics on the system response. Although interest in tension leg platforms peaked in the late 1980s, there has been a recent surge of interest to studying how these, and similar systems, behave [1, 2, 3, 4]. Historically, the motivation to study TLPs has been dominated by the oil industry; however, there has been a shift studying how these systems can be applied to lightweight floating offshore wind platforms [5, 6].

To begin the systematic design of a TLP, the first step is to assemble a dynamics model. Dynamics models can be classified into two high level groups, as defined by both the International Ships and Offshore Structure Congress (ISSC) and the American Petroleum Institute (API) [7]: uncoupled analysis and coupled analysis. Uncoupled analysis ignores the cable dynamics and drag forces by assuming the tendons behave as linear springs. Examples of such systems are plentiful [1, 2, 8, 9]. On the other hand, a coupled model represents the cables as a discretized system of masses attached to visco–elastic elements. The most common implementations use some form of the Finite Element Analysis (FEA) representation to model the tendons

[10, 11, 12, 13]. To avoid confusion, we emphasize that uncoupled/coupled analysis only refers to the manner of cables representation, and not the coupling effects that occur between degrees of freedom.

As suggested by the works surveyed [2, 8, 14], in certain circumstances, it is reasonable to replace the FEA cable with a linear spring equivalent. The idea behind the substitution is to increase simulation efficiency and speed, while maintaining accuracy. The mechanisms promoting similarity between the coupled and uncoupled models are not fully understood, though great efforts were undertaken by Mekha *et al.* [14], to study how particular cable models affect a TLP simulation. Among the observations, Mekha demonstrates that water depth increases, differences between the models are more likely. Although this work identifies the source of disagreement, the results pertain only to the specific TLP being modeled, making it difficult to characterize other platforms. Others have identified the platform–to–cable–mass ratio as a parameter gauging the significance of tendon dynamics [15, 16, 17]. The goal of the work discussed in this paper is to investigate this issue rigorously using analytical models, which can be used to interpret the characteristics portrayed in numerical models.

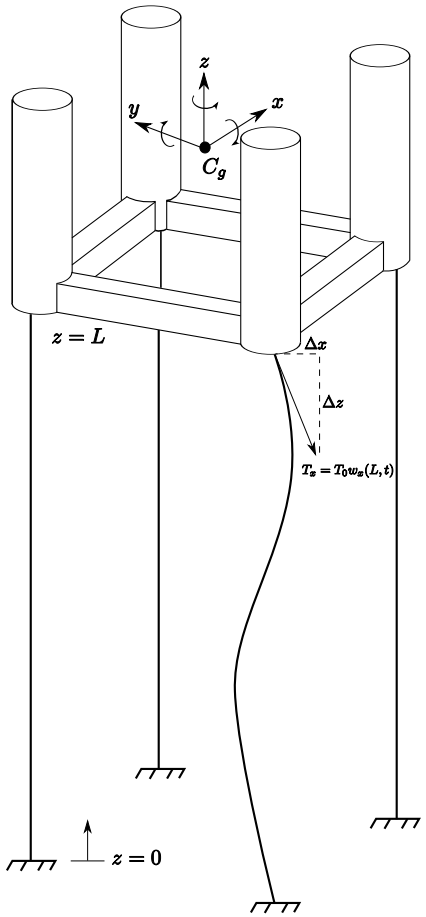

Figure 1: The analytical models derived in this work assume the TLP geometry and boundaries depicted in this figure. Variable $T_x(t)$ is the dynamic tension due to transverse oscillations, and it is aligned with the x–axis. For clarity, the profile for one tendon is shown, but it is implied that remaining tendons oscillate in a similar manner.

2 Overview of the Analysis Technique

To initiate this study, the research team derived a set of transfer functions describing the platform response for each degree of freedom. The TLP has motion in six directions: surge (x), sway (y), heave (z), roll (ϕ), pitch (θ) and yaw (ψ); but only four were modeled because sway is analogous to surge, and roll is analogous to pitch. Roll/pitch is defined as a rotation about the x/y axis, and yaw as a rotation about the z axis (Figure 1). The *coupled analytical model* is obtained by treating each tendon as a continuous system with mass subject to external (hydrodynamic) forces, and acts as a surrogate for a coupled TLP dynamics model that uses an FEA cable representation. This substitution permits a closed–form analytical solution to be obtained to predict time domain response characteristics [18, 19]. The derivation process used here is similar to that used by Grosenbaugh [18], but differs by the addition of multiple cables and use of a non-dimensional solution. For baseline comparison, an *uncoupled analytical model* is also derived. The linearized tendon restoring force in the uncoupled analytical model is based on the stiffness matrix developed by Malaeb [9].

Before proceeding, it is important to first understand the relationship between transverse and longitudinal cable vibrations, and how they react with TLP motions. Two studies chronicle theses effects; Nordgren [20] shows that high–frequency degrees of freedom, which tend to be the heave and roll/pitch directions in TLPs, are sensitive to the longitudinal tendon frequencies. This is attributed to the longitudinal cable natural frequencies approaching the heave and roll/pitch natural frequencies. Therefore, the coupled analytical models for heave and roll/pitch directions were developed while assuming that the longitudinal cable excitations are important. Dong *et al.* [21], shows the low frequency degrees of freedom (i.e., the surge/sway and yaw directions in TLPs) are more likely to respond to transverse cable disturbances. This examination of the surge/sway and yaw analytical models consider transverse cable disturbance effects, but not longitudinal vibrations. The principle assumptions used in this analysis are summarized in the following statements:

- Surge/sway and yaw platform motions excite the transverse tendon modes.
- Heave and roll/pitch platform motions excite the longitudinal tendon modes.
- The equations are obtained by linearizing the platform about a zero initial displacement.
- Motion between degrees of freedom is decoupled in order to simplify the analysis and to obtain a fundamental understanding of the mechanisms influencing the importance of tendon dynamics on the TLP response.
- In the example presented in this manuscript, the fluid damping forces are linearized quadratic drag terms [22], and the fluid added mass is a fixed coefficient. However, the method of analysis does not change if radiation damping is considered, or if the added mass is frequency dependent. In seeking a non-dimensional solution, we will show the results are independent of platform damping coefficients.

3 Coupled Analytical Model

In this section, we show the derivation of the heave coupled analytical model in a meticulous manner; this discussion provides the mathematical foundations needed to obtain the remaining degrees of freedom. The tendon is attached to the platform at $z = L$, and to the seabed at $z = 0$ (Figure 1). The function $u(z,t)$ describes the cable stretch in the z direction, and $w(z,t)$ represents the transverse amplitude (Figure 2). The motions $u(z,t)$ and $w(z,t)$ are presumed to act independently to one another. Thus, a one–dimensional wave equation is sufficient to describe the tendon motions. The function $u(z,t)$ is [23]:

$$c_z^2 u_{zz}(z,t) + \hat{g} = u_{tt}(z,t) + \frac{d_z}{\mu} u_t(z,t) \tag{1}$$

Equation 1 is used to develop the heave and roll/pitch coupled analytical models. The transverse tendon displacement, $w(z,t)$, is once again governed by a one–dimensional wave equation [23]:

$$c_x^2 w_{zz}(z,t) + \hat{g} = w_{tt}(z,t) + \frac{d_x}{\mu} w_t(z,t) \tag{2}$$

Equation 2 is used to characterize the surge/sway and yaw coupled analytical models. In the above equations, $\hat{g} = g\frac{\rho_c - \rho}{\rho}$ is the effective gravitational force per unit length after accounting for buoyancy, μ is the cable mass plus added mass per unit length, d_z and d_x give the cable damping coefficients per unit length, $c_z = [AE/\mu]^{1/2}$ and $c_x = [T_0/\mu]^{1/2}$ are the longitudinal and transverse wave speeds, respectively. In the definition for $\hat{g}$, ρ_c is the cable density in air, ρ is the density of sea water, and g is the acceleration due to gravity. The expression u_{ij} denotes the second partial derivative $u_{ij} = \frac{\partial^2 u}{\partial i \partial j}$. Variable T_0 is the tendon pretension and AE is its axial stiffness. For a circular cable element, the fluid added mass is equal to the mass of the fluid being displaced; thus $\mu = A(\rho_c + \rho)$ [26]. It is assumed the cable properties are constant along the length of the cable. Tangential viscous forces along the cable are omitted since these are small compared to the longitudinal cable tension [18, 19]. All linearized coefficients (such as d_x and D_i, which is introduced later) are obtained using the Caughey linearization technique [22].

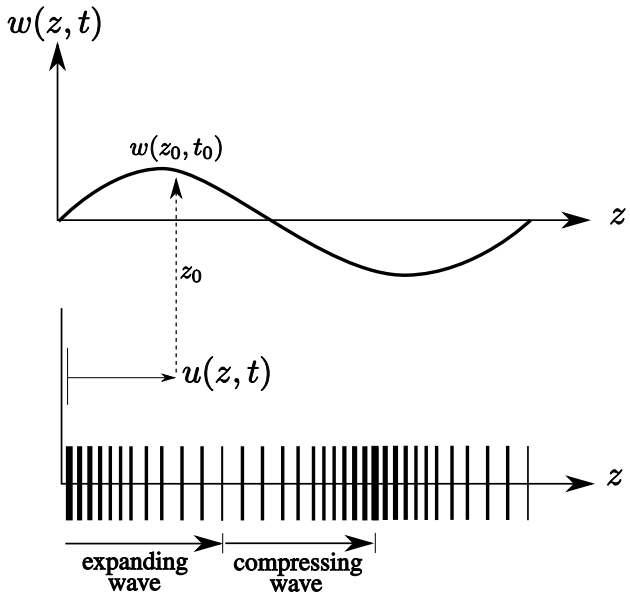

Figure 2: In the coupled analytical TLP model, each tendon is permitted to deform in the manner pictured. $u(z,t)$ represents the cable stretch in the longitudinal direction, and $w(z,t)$ is a displacement in a direction normal to the z-axis and represents transverse motions.

3.1 Heave Analytical Model

Coupling of the platform and cable dynamics is accomplished by solving Equation 1 with the platform equation of motion acting as a boundary condition. Recognizing that the platform motion is identical to the tendon motion at $u(L,t)$, the TLP equation of motion in the heave direction is:

$$M_z u_{tt}(L,t) + D_z u_t(L,t) = \bar{B}(t) - M_{tlp} g - \bar{T}_z(t) \tag{3}$$

Variable $\bar{T}_z(t) = 4T_0 + 4T_z(t)$ is a sum of the initial cable pretension and the time–varying tension $T_z(t)$, and $\bar{B}(t) = B_0 + B(t)$ is the static buoyancy B_0 plus dynamic buoyancy $B(t)$. The remaining terms are defined as: M_z is a sum of the platform mass (M_{tlp}) and added mass; L is the tendon length; D_z is the linearized platform damping coefficient in the heave direction. It follows that, with the platform in static equilibrium:

$$B_0 - M_{tlp} g - 4T_0 = 0 \tag{4}$$

The dynamic buoyancy is:

$$B(t) = K_z \{Y(t) - u(L,t)\} = F_z(t) - K_z u(L,t) \tag{5}$$

where $K_z = 4g\rho A_c$ represents the buoyancy stiffness, A_c is the column cross–sectional area, and $F_z(t)$ is the varying heave force due to the wave height $Y(t) = He^{j\omega t}$. After substitution, the final form of Equation 3 is:

$$M_z u_{tt}(L,t) + D_z u_t(L,t) + K_z u(L,t) + 4T_z(t) = F_z(t) \tag{6}$$

where

$$T_z(t) = AEu_z(L,t) \tag{7a}$$

Equation 7a is the upper boundary condition that completes the platform/cable coupling. The lower boundary condition (i.e., at the tnedon base) is simply:

$$u(0,t) = 0 \tag{7b}$$

3.1.1 Non–Dimensionlization of the Heave Model

For generality, the problem is non–dimensionalized to identify the important cable parameters influencing the system response. This introduces the following dimensionless terms:

$$z = L\tilde{z} \qquad t = \frac{L}{c_z}\tilde{t} \qquad u = H\tilde{u}(\tilde{z},\tilde{t}) \qquad \omega = \frac{c_z}{L}\tilde{\omega}$$

This results in the following synthesis of Equations 1 and 6:

$$\text{Longitudinal Wave Eqn.} \qquad \tilde{u}_{zz}(\tilde{z},\tilde{t}) + \frac{L^2}{c_z^2 H}\hat{g} = \tilde{u}_{tt}(\tilde{z},\tilde{t}) + \frac{Ld_z}{\mu c_z}\tilde{u}_t(\tilde{z},\tilde{t}) \tag{8a}$$

$$\text{Heave EOM} \qquad \frac{M_z}{4\mu L}\tilde{u}_{tt}(1,\tilde{t}) + \frac{D_z}{4\mu c_z}\tilde{u}_t(1,\tilde{t}) + \frac{K_z L}{4AE}\tilde{u}(1,\tilde{t}) + \tilde{u}_z(1,\tilde{t}) = \frac{LF_z(t)}{4AEH} \tag{8b}$$

3.1.2 Solution to the Heave Coupled Model

The preceding equations are used to obtain the transfer function $\tilde{G}_z(\tilde{s}) = \frac{\tilde{U}(1,\tilde{s})}{\tilde{F}_z(\tilde{s})}$, which relates the heave motion response with respect to the vertical wave force. Before solving the problem, the time variable in the governing partial differential equation is removed by virtue of the Laplace transformation [18, 19, 25]. Equation 8a is:

$$\tilde{U}''(\tilde{z},\tilde{s}) + \frac{L^2}{c_z^2 H}\hat{g} = \tilde{s}^2\tilde{U}(\tilde{z},\tilde{s}) + \tilde{s}\frac{Ld_z}{\mu c_z}\tilde{U}(\tilde{z},\tilde{s}) \tag{9}$$

where $\tilde{s}$ is the complex frequency $j\tilde{\omega}$, and $\tilde{U}''(\tilde{z},\tilde{s})$ represents the second derivative of $\tilde{U}(\tilde{z},\tilde{s})$ with respect to $\tilde{z}$. Equation 9 is a non–homogeneous differential equation, and the solution to this problem is:

$$U(z,s) = \underbrace{C_1 e^{\tilde{k}_z(\tilde{s})\tilde{z}} + C_2 e^{-\tilde{k}_z(\tilde{s})\tilde{z}}}_{\text{CF}} - \underbrace{\beta(\tilde{s})}_{\text{PI}} \tag{10}$$

where the elastic wave number $\tilde{k}_z(\tilde{s})$ is equal to:

$$\tilde{k}_z(\tilde{s}) = \sqrt{\tilde{s}^2 + \tilde{s}\frac{Ld_z}{\mu c_z}} \tag{11}$$

CF is the complementary function and PI is the particular integral. The boundary conditions, Equations 7a and 7b, are transformed into their dimensionless equivalent to find a solution for Equation 9:

$$\tilde{U}(0,\tilde{s}) = 0 \tag{12a}$$

$$\tilde{U}'(1,\tilde{s}) = \frac{L\mathcal{T}_z(\tilde{s})}{AEH} \tag{12b}$$

where $\mathcal{T}_z(\tilde{s})$ is the tension at $z = L$. The complementary function is solved by setting $\frac{L^2}{c_z^2 H}\hat{g}$ in Equation 9 to zero, then solving for $\beta(\tilde{s})$. With $\beta(\tilde{s})$ now known and $\frac{L^2}{c_z^2 H}\hat{g}$ inserted back into the equation, the coefficients

C_1 and C_2 are determined. The solution to the particular integral is not of interest for a reason that will become apparent shortly. However, for completeness, the value of $\beta(\tilde{s})$ is stated as:

$$\beta(\tilde{s}) = \frac{\frac{L^2}{c_z^2 H}\hat{g}}{\tilde{s}^2 + \tilde{s}\frac{Ld_z}{\mu c_z}}$$

The complete solution to Equation 9 is:

$$\tilde{U}(\tilde{z},\tilde{s}) = \left\{ \frac{\frac{L\mathcal{T}_z(\tilde{s})}{AEH\tilde{k}_z(\tilde{s})}e^{\tilde{k}_z(\tilde{s})} + \beta(\tilde{s})}{e^{2\tilde{k}_z(\tilde{s})}+1} \right\} e^{\tilde{k}_z(\tilde{s})\tilde{z}} + \left\{ \frac{\beta(\tilde{s})e^{\tilde{k}_z(\tilde{s})} - \frac{L\mathcal{T}_z(s)}{AEH\tilde{k}_z(\tilde{s})}}{2\cosh\left\{\tilde{k}_z(\tilde{s})\right\}} \right\} e^{-\tilde{k}_z(\tilde{s})\tilde{z}} - \beta(\tilde{s}) \tag{13}$$

Isolating $\mathcal{T}_z(\tilde{s})$ in Equation 13 gives the tension at the top of the tendon:

$$\mathcal{T}_z(\tilde{s}) = \frac{AEH\tilde{k}_z(\tilde{s})}{L\tanh\left\{\tilde{k}_z(\tilde{s})\right\}}\tilde{U}(1,\tilde{s}) - \mathcal{T}_z(\tilde{s})\frac{\beta(\tilde{s})}{\sinh\left\{\tilde{k}_z(\tilde{s})\right\}} \tag{14}$$

Ideally, a transfer function describing the TLP displacement is desired. This is achieved by applying a Laplace transformation on Equation 8b, then inserting Equation 14 into this equation. This results in:

$$\tilde{F}_z(\tilde{s}) + \frac{\beta(\tilde{s})}{\sinh\left\{\tilde{k}_z(\tilde{s})\right\}} = \tilde{U}(1,\tilde{s})\left[\tilde{s}^2\frac{M_z}{4\mu L} + \tilde{s}\frac{D_z}{4\mu c_z} + \frac{K_z L}{4AE} + \frac{\tilde{k}_z(\tilde{s})}{\tanh\left\{\tilde{k}_z(\tilde{s})\right\}}\right] \tag{15}$$

Since $\frac{\beta(\tilde{s})}{\sinh\left\{\tilde{k}_z(\tilde{s})\right\}}$ is independent of the input $\tilde{F}_z(\tilde{s})$ and the output $\tilde{U}(1,\tilde{s})$, it is disregarded as part of the desired transfer function. The transfer function describing the heave motion now appears in its final form:

$$\tilde{G}_z(\tilde{s}) = \frac{\tilde{U}(1,\tilde{s})}{\tilde{F}_z(\tilde{s})} = \frac{1}{\tilde{s}^2\frac{M_z}{4\mu L} + \tilde{s}\frac{D_z}{4\mu c_z} + \frac{K_z L}{4AE} + \frac{\tilde{k}_z(\tilde{s})}{\tanh\left\{\tilde{k}_z(\tilde{s})\right\}}} \tag{16}$$

The dimensionless vertical wave force is:

$$\tilde{F}_z(\tilde{s}) = \frac{LF_z(\tilde{s})}{4AEH} \tag{17}$$

3.2 The Remaining Degrees of Freedom

For brevity, the following sections present the differential equations and governing conditions used to assemble the remaining coupled analytical models. Each degree of freedom is analyzed and solved in a manner consistent to the heave direction. For the roll/pitch and yaw directions, the following normalized terms must be considered:

$$\theta(t) = \frac{2H}{L_a}\tilde{\theta}(\tilde{t}) \qquad \psi(t) = \frac{H}{L_b}\tilde{\psi}(\tilde{t})$$

where L_a is the lateral distance between adjacent tendon attachment points and L_b is the distance from the TLP center of gravity and tendon attachment point in the xy plane. The transverse tendon displacement must also be non–dimensionalized:

$$w = H\tilde{w}(\tilde{z},\tilde{t})$$

When considering surge/sway and yaw degree of freedom, different dimensionless time and frequency variables must be used since the transverse tendon oscillations are important:

$$t = \frac{L}{c_x}\tilde{t} \qquad \omega = \frac{c_x}{L}\tilde{\omega}$$

3.2.1 Surge/Sway Coupled Model

The dynamic tension in the surge/sway direction is:

$$T_0 w_z(L,t) = T_x(t) \tag{18a}$$

Figure 1 assists in the physical description of Equation 18a. It is assumed the pretension T_0 is fixed with respect to time and length along the cable. At the seabed, the tendon is fixed and immovable; therefore:

$$w(0,t) = 0 \tag{18b}$$

Both Equations 18a and 18b combine to form the boundary conditions in the surge/sway directions. The forces acting on the platform are a result of the four tendons $4T_x(t)$, the surge hydrodynamic resistance coefficient D_x, and a surge wave excitation force $F_x(t)$. The coupled equation of motion for the platform in the surge direction is:

$$M_x w_{tt}(L,t) + D_x w_t(L,t) + 4T_0 w_z(L,t) = F_x(t) \tag{19}$$

where M_x is the summation of the structural and added mass. In dimensionless form, the expressions used to solve the coupled surge/sway analytical model are:

$$\text{Transverse Wave Eqn.} \qquad \tilde{w}_{zz}(\tilde{z},\tilde{t}) = \tilde{w}_{tt}(\tilde{z},\tilde{t}) + \frac{Ld_x}{\mu c_x}\tilde{w}_t(\tilde{z},\tilde{t}) \tag{20a}$$

$$\text{Surge/Sway EOM} \qquad \frac{M_x}{4\mu L}\tilde{w}_{tt}(1,\tilde{t}) + \frac{D_x}{4\mu c_x}\tilde{w}_t(1,\tilde{t}) + \tilde{w}_z(1,\tilde{t}) = \frac{LF_x(t)}{4T_0 H} \tag{20b}$$

The effects of gravity $\hat{g}$ is removed from Equation 20a since it is not important to the final solution. This results in:

$$\tilde{G}_x(\tilde{s}) = \frac{\tilde{W}(1,\tilde{s})}{\tilde{F}_x(\tilde{s})} = \frac{1}{\tilde{s}^2\frac{M_x}{4\mu L} + \tilde{s}\frac{D_x}{4\mu c_x} + \frac{\tilde{k}_x(\tilde{s})}{\tanh\{\tilde{k}_x(\tilde{s})\}}} \tag{21}$$

where the dimensionless elastic wave number $\tilde{k}_x(\tilde{s})$ is:

$$\tilde{k}_x(\tilde{s}) = \sqrt{\tilde{s}^2 + \tilde{s}\frac{Ld_x}{\mu c_x}} \tag{22}$$

3.2.2 Roll/Pitch Coupled Model

A pitch displacement $\theta(t)$ also induces a displacement at the end of the tendon according to $\frac{L_a}{2}\theta(t) = u(L,t)$. This leads to the following normalized relationship:

$$H\tilde{u}(1,\tilde{t}) = \frac{L_a}{2}\frac{2H}{L_a}\tilde{\theta}(t) \qquad \Rightarrow \qquad \tilde{U}(1,\tilde{s}) = \tilde{\Theta}(\tilde{s})$$

The equation of motion in the roll/pitch direction is:

$$I_{xx}\ddot{\theta}(t) + D_\theta\dot{\theta}(t) + K_\theta\theta(t) + \underbrace{4\left(\bar{h}T_0\theta(t) + \frac{1}{2}L_a T_z(t)\right)}_{\text{Dynamic Tendon Moment}} = M_\theta(t) \tag{23}$$

where I_{xx} is the platform mass moment of inertia, including the added mass moment of inertia, in seawater. The dynamic tendon moment is solved by summing all individual cable moments about the platform's center of gravity, $M_\theta(t)$ is the wave moment in the roll/pitch direction, $K_\theta = \rho g I_{00}$ is the buoyant righting moment [9], and I_{00} is the second moment of area where the waterline intersects the TLP. Variable $\bar{h}$ is the vertical distance from the center of gravity to the tendon attachment point. The roll/pitch coupled analytical model is developed using:

$$\text{Longitudinal Wave Eqn.} \qquad \tilde{u}_{zz}(\tilde{z},\tilde{t}) = \tilde{u}_{tt}(\tilde{z},\tilde{t}) + \frac{Ld_z}{\mu c_z}\tilde{u}_t(\tilde{z},\tilde{t}) \tag{24a}$$

$$\text{Roll/Pitch EOM} \qquad \frac{I_{xx}}{L_a^2\mu L}\tilde{\theta}_{tt}(\tilde{t}) + \frac{D_\theta}{L_a^2\mu c_z}\tilde{\theta}_t(\tilde{t}) + \left(\frac{K_\theta L + 4\bar{h}T_0 L}{L_a^2 AE}\right)\tilde{\theta}(\tilde{t}) + \tilde{u}_z(1,\tilde{t}) = \frac{LM_\theta(t)}{2L_a AEH} \tag{24b}$$

The solution to Equation 24a and 24b is:

$$\tilde{G}_\theta(\tilde{s}) = \frac{\tilde{\Theta}(\tilde{s})}{\tilde{M}_\theta(\tilde{s})} = \frac{1}{\tilde{s}^2 \frac{I_{xx}}{L_a^2 \mu L} + \tilde{s} \frac{D_\theta}{L_a^2 \mu c_z} + \frac{K_\theta L + 4\bar{h} T_0 L}{L_a^2 AE} + \frac{\tilde{k}_z(\tilde{s})}{\tanh\{\tilde{k}_z(\tilde{s})\}}} \tag{25}$$

3.2.3 Yaw Coupled Model

The platform yaw equation of motion is:

$$I_{zz}\ddot{\psi}(t) + D_\psi \dot{\psi}(t) + 4L_b T_x(t) = M_\psi(t) \tag{26}$$

The transverse wave equation, Equation 2, is used to solve the yaw coupled analytical model. In dimensionless form, the equations solved are:

$$\text{Transverse Wave Eqn.} \qquad \tilde{w}_{zz}(\tilde{z},\tilde{t}) = \tilde{w}_{tt}(\tilde{z},\tilde{t}) + \frac{Ld_x}{\mu c_x}\tilde{w}_t(\tilde{z},\tilde{t}) \tag{27a}$$

$$\text{Yaw EOM} \qquad \frac{I_{zz}}{4L_b^2 \mu L}\tilde{\psi}_{tt}(\tilde{t}) + \frac{D_\psi}{4L_b^2 \mu c_x}\tilde{\psi}_t(\tilde{t}) + \tilde{w}_z(1,\tilde{t}) = \frac{LM_\psi(t)}{4L_b T_0 H(t)} \tag{27b}$$

The solution is:

$$\tilde{G}_\psi(\tilde{s}) = \frac{\tilde{\Psi}(\tilde{s})}{\tilde{M}_\psi(\tilde{s})} = \frac{1}{\tilde{s}^2 \frac{I_{zz}}{4L_b^2 \mu L} + \tilde{s} \frac{D_\psi}{4L_b^2 \mu c_x} + \frac{\tilde{k}_x(\tilde{s})}{\tanh\{\tilde{k}_x(\tilde{s})\}}} \tag{28}$$

3.3 Coupled Model Summary

The non–dimensional transfer functions, which are given in Equations 16, 21, 25, and 28, all have the form:

$$\tilde{G}_i(\tilde{s}) = \frac{1}{\tilde{s}^2\Gamma_i + \tilde{s}\Pi_i + \Omega_i + \frac{\sqrt{\tilde{s}^2 + \tilde{s}\Lambda_i}}{\tanh\{\sqrt{\tilde{s}^2 + \tilde{s}\Lambda_i}\}}} \tag{29}$$

where Γ_i, Π_i, Ω_i, and Λ_i are dimensionless coefficients representing the following:

- Γ_i is the platform/cable mass ratio
- Π_i is the platform drag/elastic cable force ratio
- Ω_i is the platform buoyancy/cable stiffness ratio
- Λ_i is the dissipative/elastic cable force ratio

Table 2 gives the values for the dimensionless coefficients based on the model implemented in Malaeb [9], but with the platform at two operating depths: $d = 600$ meters and $d = 1200$ meters. The platform properties are outlined in Table 1.

4 Uncoupled Analytical Model

The uncoupled analytical TLP model serves as a benchmark for comparing model differences. This helps clarify how tendon properties influence TLP responses. Less effort is required to derive this model because cable dynamics are neglected, effectively rendering the TLP to a mass–spring–damper system. The transfer functions are obtained by linearizing the tendon forces about the platform equilibrium position. For generalized coordinates $q_i = \{x, z, \theta, \psi\}$, the linearized equation of motion is:

$$M_i\ddot{q}_i(t) + D_i\dot{q}_i(t) + C_i q_i(t) = F_i(t) \tag{30}$$

C_i is the linearized tendon stiffness for the i^{th} degree of freedom obtained by linearizing Malaeb's stiffness matrix about the platform equilibrium [9]. Buoyancy stiffness is also accounted for in K_z (for heave) and

Table 1: TLP Physical Properties

Property		Value
D	- Column Diameter	16 m
L_a	- Pontoon Length	60 m
L_b	- Distance from C_g to Column	42.4 m
L_c	- Equilibrium Submerged Column Length	33 m
L_p	- Pontoon Width/Height	8.86 m
$\bar{h}$	- Height of C_g Above Platform Base	31 m
T_{tot}	- Total Pretension	1x10^8 N
M_{tlp}	- Platform Mass in Air	3.466x10^7 kg
I_{xx}	- Moment of Inertia About x-axis	8.45x10^{10} kg·m^2
I_{yy}	- Moment of Inertia About y-axis	8.45x10^{10} kg·m^2
I_{zz}	- Moment of Inertia About z-axis	1.02x10^{11} kg·m^2
ρ_c	- Cable Density in Air	6500 kg/m^3
A	- Cable Cross Sectional Area per Corner	0.1982 m^2
E	- Cable Modulus of Elasticity	180 GPa

K_θ (for pitch). This process is applied to each degree of freedom. The dimensionless uncoupled analytical model bears the following form:

$$\tilde{H}_i(s) = \frac{1}{(\tau_i s)^2 + \zeta_i \tau_i s + 1} \tag{31}$$

where the coefficients τ_i and ζ_i are:

$$\tau_i = \sqrt{\frac{M_i}{C_i}} \qquad \zeta_i = \frac{D_i}{\sqrt{M_i C_i}}$$

Values for coefficients τ_i and ζ_i are given in Table 3. Note that the dominant TLP natural frequency is the reciprocal of τ_i, i.e. TLP natural frequency $= \tau_i^{-1}$, so it has units of seconds per radian.

5 Parameter Sensitivity

The uncoupled and coupled models are identical when transfer functions $\tilde{G}_i(\tilde{s})$ and $\tilde{H}_i(s)$ are that same. An examination comparing the similarities of $\tilde{G}_i(\tilde{s})$ and $\tilde{H}_i(s)$ can be performed two ways. Method one involves plotting both transfer functions, then through a visual inspection, noting the differences between them. This is a subjective method, requiring all coefficients in Table 2 and Table 3 to be readily known. The second method evaluates the coupled and uncoupled transfer functions algebraically. A benefit of this technique is that it eliminates the linearized hydrodynamic coefficients D_i from the process, which results in less effort required to perform the analysis. For complex sub–sea geometries, calculating the linearized drag coefficients D_i can become difficult.

5.1 Visual Relationships

To assist our understanding of the dynamic characteristics, the Bode plots of Equations 29 and 31 are given in Figure 3. Because these models are expressed non–dimensionally, the roll/pitch and yaw directions adopt similar behaviors and characteristics. The wave band frequency, defined as the region where 90% of the wave energy is concentrated, is also shown. Based on these figure, the following observations are noted:

1. The plots show strong agreement between the coupled and uncoupled models at low frequencies up to the wave band frequencies. This reinforces observations made in the literature [14]. Disagreements be-

Table 2: Coupled TLP analytical model dimensionless coefficients

Degree of Freedom	Γ_i	Π_i	Ω_i	Λ_i
$\tilde{G}_x(\tilde{s})$	$\frac{M_x}{4\mu L}$	$\frac{D_x}{4\sqrt{\mu T_0}}$	–	$\frac{Ld_x}{\sqrt{\mu T_0}}$
(at depth = 600 m)	12.86	1.62		2.73
(at depth = 1200 m)	6.43	1.62		5.45
$\tilde{G}_z(\tilde{s})$	$\frac{M_z}{4\mu L}$	$\frac{D_z}{4\sqrt{\mu AE}}$	$\frac{K_z L}{4AE}$	$\frac{Ld_z}{\sqrt{\mu AE}}$
(at depth = 600 m)	11.13	0.49	0.034	2.05×10^{-4}
(at depth = 1200 m)	5.56	0.49	0.068	4.11×10^{-4}
$\tilde{G}_\theta(\tilde{s})$	$\frac{I_{xx}}{L_a^2\mu L}$	$\frac{D_\theta}{L_a^2\sqrt{\mu AE}}$	$\frac{K_\theta L+4\bar{h}T_0 L}{L_a^2 AE}$	$\frac{Ld_z}{\sqrt{\mu AE}}$
(at depth = 600 m)	34.86	2.15	0.046	2.05×10^{-4}
(at depth = 1200 m)	17.43	2.15	0.093	4.11×10^{-4}
$\tilde{G}_\psi(\tilde{s})$	$\frac{I_{zz}}{4L_b^2\mu L}$	$\frac{D_\psi}{4L_b^2\sqrt{\mu T_0}}$	–	$\frac{Ld_x}{\sqrt{\mu T_0}}$
(at depth = 600 m)	22.90	3.22		2.73
(at depth = 1200 m)	11.45	3.22		5.45

tween models appear at longitudinal cable natural frequencies in the heave response. These disparities appear at increments of $\tilde{\omega}_{x,z}^n = n\pi$, where $n = 1, 2, \cdots$.

2. Λ_i governs the amplitude of the peaks located at $\tilde{\omega}_{x,z}^n$. When $\Lambda_i < 1$, the amplitudes at $\tilde{\omega}_{x,z}^n$ are large, which implies the damping coefficient d_i is small and the cable itself cannot dissipate energy propagating along the tendon. As a result, the residual energy is transferred to the platform. This is evident by the heave responses in Figure 3. The cable cannot completely dissipate longitudinal energy, which makes the platform sensitive to high frequency disturbances. This agrees with principles outlined in [10, 13].

3. When $\Lambda_i > 1$, d_i is large, the tendon will provide supplementary damping (that is, damping in addition to D_i) to the platform. As exemplified in [14], this effect is most likely to be observed in surge/sway and yaw. The transverse cable damping d_x is a result of viscous drag in the cross–flow direction, which will slow the platform progression and limit the amplitudes of oscillation. Figure 3(b) illustrates subtle evidence of this, where the peak amplitude of $\tilde{G}_x(\tilde{s})$ is less than $\tilde{H}_x(s)$.

4. As water depth increases, the tendon natural frequencies approach the wave band frequencies, presenting a proclivity for tether excitation.

This study demonstrates, through graphical interpretations, the manner in which the tendon dynamics will influence the TLP response. Additional factors, which are not apparent from this analysis, are also important. The next section outlines the criteria that must be achieved to preserve agreement between the two models.

5.2 Algebraic Relationships

It is understood the uncoupled and coupled transfer functions behave identically when $\tilde{G}_i(\tilde{s}) = \tilde{H}_i(s)$. Thus:

$$\tilde{s}^2\Gamma_i + \tilde{s}\Pi_i + \Omega_i + \frac{\sqrt{\tilde{s}^2 + \tilde{s}\Lambda_i}}{\tanh\left\{\sqrt{\tilde{s}^2 + \tilde{s}\Lambda_i}\right\}} = (\tau_i s)^2 + \zeta_i\tau_i s + 1 \tag{32}$$

Table 3: Uncoupled TLP analytical model dimensionless coefficients

Degree of Freedom	τ_i	ζ_i
$\tilde{H}_x(s)$	$\sqrt{\frac{M_x L}{4T_0}}$ s/rad	$D_x\sqrt{\frac{L}{4M_x T_0}}$
(at depth = 600 m)	17.72	0.45
(at depth = 1200 m)	25.10	0.64
$\tilde{H}_z(s)$	$\sqrt{\frac{M_z L}{K_z L+4AE}}$ s/rad	$D_z\sqrt{\frac{L}{M_z(K_z L+4AE)}}$
(at depth = 600 m)	0.40	0.14
(at depth = 1200 m)	0.56	0.20
$\tilde{H}_\theta(s)$	$\sqrt{\frac{I_{xx} L}{K_\theta L+4\bar{h}T_0 L+L_a^2 AE}}$ s/rad	$D_\theta\sqrt{\frac{L}{I_{xx}(K_\theta L+4\bar{h}T_0 L+L_a^2 AE)}}$
(at depth = 600 m)	0.71	0.36
(at depth = 1200 m)	0.98	0.49
$\tilde{H}_\psi(s)$	$\sqrt{\frac{I_{zz} L}{4L_b^2 T_0}}$ s/rad	$D_\psi\sqrt{\frac{L}{4I_{zz}(L_b^2 T_0)}}$
(at depth = 600 m)	23.64	0.34
(at depth = 1200 m)	33.44	0.48

Or, equivalently,

$$\left[\Gamma_i - \left(\frac{c_i}{L}\right)^2 \tau_i^2\right]\tilde{s}^2 + \left[\Pi_i - \left(\frac{c_i}{L}\right)\zeta_i\tau_i\right]\tilde{s} + [\Omega_i - 1] + \frac{\sqrt{\tilde{s}^2+\tilde{s}\Lambda_i}}{\tanh\left\{\sqrt{\tilde{s}^2+\tilde{s}\Lambda_i}\right\}} = 0 \tag{33}$$

Values for the heave direction are inserted into Equation 33 to produce:

$$\Gamma_z - \left(\frac{c_z}{L}\right)^2 \tau_z^2 \quad \Rightarrow \quad \frac{4AE}{K_z L+4AE} = 1 \tag{34a}$$

$$\Pi_z - \left(\frac{c_z}{L}\right)\zeta_z\tau_z \quad \Rightarrow \quad \frac{4AE}{K_z L+4AE} = 1 \tag{34b}$$

$$\Omega_z - 1 + \frac{\sqrt{\tilde{s}^2+\tilde{s}\Lambda_z}}{\tanh\left\{\sqrt{\tilde{s}^2+\tilde{s}\Lambda_x}\right\}} \quad \Rightarrow \quad \frac{K_z L}{4AE} + \frac{\sqrt{\tilde{s}^2+\tilde{s}\Lambda_z}}{\tanh\left\{\sqrt{\tilde{s}^2+\tilde{s}\Lambda_z}\right\}} = 1 \tag{34c}$$

The requirement governing Equations 34a and 34b are identical, and are achieved only if $K_z L \ll 4AE$, which is a condition less obvious through graphical interpretation. A small K_z compared to a large $4AE/L$ has the effect of reducing platform heave sensitivity to wave height fluctuations, which in turn limits cable tension variations. If the criteria in Equation 34a/34b is met, Equation 34c reduces to the following relation since $\frac{K_z L}{4AE} \approx 0$:

$$\frac{\sqrt{\tilde{s}^2+\tilde{s}\Lambda_z}}{\tanh\left\{\sqrt{\tilde{s}^2+\tilde{s}\Lambda_z}\right\}} = 1 \tag{35}$$

Equation 35 cannot be satisfied since it is a frequency–varying function. There are, however, instances when the tendon dynamics can be deemed negligible, which renders Equation 35 insignificant. As outlined earlier, this is most likely when $\Lambda_z = 1$.

5.2.1 The Consequences of Λ_i

Figure 4 illustrates the left–hand side of Equation 35 with Λ_i varying between 0.001 and 100. When $\Lambda_i < 1$, the plot exhibits peaks appearing at intervals of $\pi(2n-1)/2$, and troughs appearing at intervals of πn.

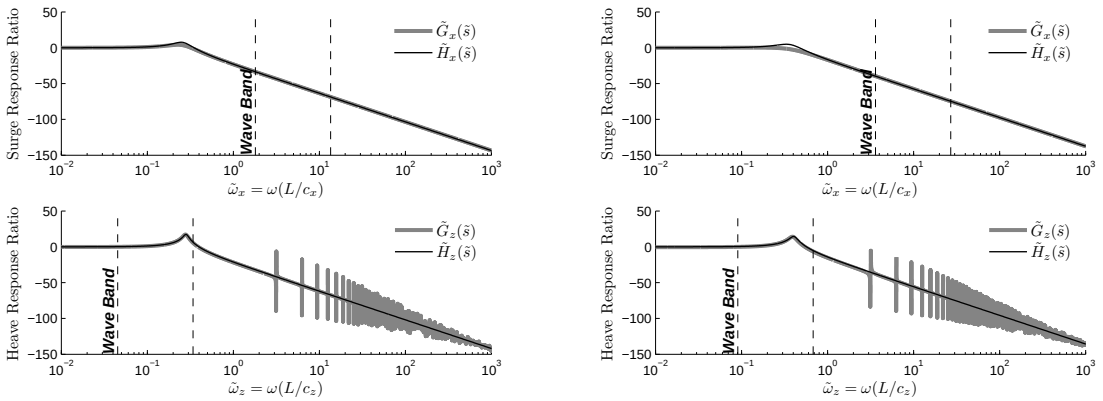

(a) Depth = 600 m

(b) Depth = 1200 m

Figure 3: The non–dimensionalized TLP surge and heave responses of a TLP in (a) 600 meters depth and (b) 1200 meters depth. This figure depicts both the coupled analytical model $\tilde{G}_{x,z}(\tilde{s})$ and the uncoupled analytical model $\tilde{H}_{x,z}(\tilde{s})$.

Troughs occur at tendon natural frequencies. As Λ_i increases, the peak amplitudes decrease, and the tendon provides an added source of damping to the TLP. When $\Lambda_i > 1$, the result is a leftward shift in the critical frequency. The critical frequency is defined as the frequency where $\frac{\sqrt{\tilde{s}^2+\tilde{s}\Lambda_i}}{\tanh\left\{\sqrt{\tilde{s}^2+\tilde{s}\Lambda_i}\right\}}$ begins a downward trend. As this frequency approaches the platform natural frequency, the TLP will change its response characteristics and begin adopting a 'damped' response. The critical frequency is determined by finding the roots of the numerator in Equation 35:

$$\sqrt{\tilde{s}^2 + \Lambda_i \tilde{s}} = 1 \tag{36}$$

There are two roots for the critical frequency $\tilde{\omega}_i^c$, but only one root is real:

$$\tilde{\omega}_i^c = \frac{-\Lambda_i + \sqrt{\Lambda_i^2 + 4}}{2} \tag{37}$$

If $d_i L$ is large relative to $\sqrt{\mu T_0}$ or $\sqrt{\mu AE}$, cable damping effects are important and their influence is reflected in the TLP response curves. This materializes when $\frac{L}{c}\tau_i^{-1} > \tilde{\omega}_i^c$ is satisfied (which is occurring in the surge response of Figure 3b), implying transverse cable motions can provide supplemental damping to the platform.

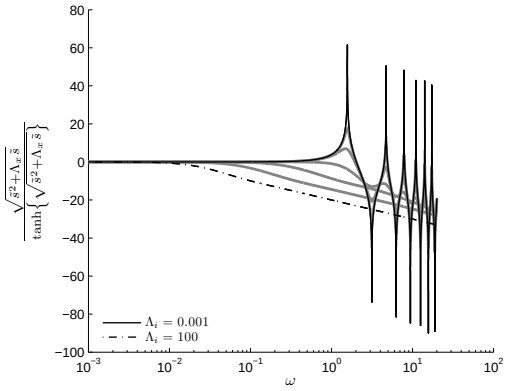

Figure 4: When Λ_i is a small number, the platform senses the longitudinal/transverse tendon motions. In the opposite case, the mooring line provides additional damping in the platform.

5.2.2 Summary for the Remaining Degrees of Freedom

Calculations equivalent to Equations 34a–34c are performed for the remaining degrees of freedom, with the results presented in Table 4. The coefficients for a TLP at $d = 600$ and $d = 1200$ meters water depth is given using the platform properties defined in Table 1.

The first condition, the *Tendon Force Condition*, arises from the Λ_i term. This quantity can also be viewed as the ratio of dissipative capacity–to–internal cable energy. When this term is equal to 1, the cable can effectively dissipate the energy contained within it. In practice, this is rarely achieved. For cases $\Lambda_i > 1$, the tendons provide extra damping to the platform, which may lead to a reduced oscillation amplitude; this is likely to occur for the surge/sway and yaw degrees of freedom. When $\Lambda_i < 1$, the platform will respond to the natural frequencies of the tendon, because the cable cannot dissipate its internal energy in that direction. This is likely to occur for the heave and roll/pitch degrees of freedom.

The second condition shown in Table 4, the *Frequency Condition*, ensures the platform is not responding to surplus cable damping. This is the criteria containing platform mass as a property, which is embedded in τ_i^{-1}. In typical TLP systems where M_i is large, the dominant natural frequency of the surge/sway (τ_x^{-1}) and yaw (τ_ψ^{-1}) are low. Therefore, it normally follows that $\frac{L}{c_x}\tau_x^{-1} < \tilde{\omega}_x^c$ and $\frac{L}{c_x}\tau_\psi^{-1} < \tilde{\omega}_x^c$. As platform mass decreases or water depth increases, the TLP will become increasingly aware of the tendon damping effects.

The third condition, the *Stiffness Condition*, measures the relative stiffness of the tendons in relation to the buoyancy stiffness. As the tendon stiffness increases, the likelihood for the coupled and uncoupled models to agree increases. Differences between the two systems typically appear when the buoyant spring stiffness exceeds the tendon stiffness by 5% or greater, i.e $\Omega_z = \frac{K_z L}{4AE} > 0.05$. This estimation is based on a parametric sweep of the deployment depth on the TLP model illustrated next.

Table 4: Criterion promoting agreement between a coupled and an uncoupled TLP model

Degree of Freedom	Tendon Force Condition	Frequency Condition	Stiffness Condition
Surge – x	$\frac{Ld_x}{\sqrt{\mu T_0}} \geq 1$	$\frac{L}{c_x}\tau_x^{-1} < \tilde{\omega}_x^c$	None
(at depth = 600 m)	$2.73 > 1$	0.27<0.33	–
(at depth = 1200 m)	$5.45 > 1$	0.39>0.17 (violation)	–
Heave – z	$\frac{Ld_z}{\sqrt{\mu AE}} \geq 1$	$\frac{L}{c_z}\tau_z^{-1} < \tilde{\omega}_z^c$	$\frac{K_z L}{4AE} \ll 1$
(at depth = 600 m)	$2.05\times10^{-4} < 1$ (violation)	0.30<0.99	0.034 < 1 (weak violation)
(at depth = 1200 m)	$4.11\times10^{-4} < 1$ (violation)	0.44<0.99	0.068 < 1 (strong violation)
Pitch – θ	$\frac{Ld_z}{\sqrt{\mu AE}} \geq 1$	$\frac{L}{c_z}\tau_\theta^{-1} < \tilde{\omega}_z^c$	$\frac{K_\theta L + 4\bar{h}T_0 L}{4L_a^2 AE} \ll 1$
(at depth = 600 m)	$2.05\times10^{-4} < 1$ (violation)	0.17<0.99	0.046 < 1 (weak violation)
(at depth = 1200 m)	$4.11\times10^{-4} < 1$ (violation)	0.25<0.99	0.093 < 1 (strong violation)
Yaw – ψ	$\frac{Ld_x}{\sqrt{\mu T_0}} \geq 1$	$\frac{L}{c_x}\tau_\psi^{-1} < \tilde{\omega}_x^c$	None
(at depth = 600 m)	$2.73 > 1$	0.21<0.33	–
(at depth = 1200 m)	$5.45 > 1$	0.30>0.18 (violation)	–

6 Case Studies

To demonstrate the cases outlined in Table 4 further, the team performed simulations of the two TLP systems. Implementation details of the coupled and uncoupled TLP dynamics models can be found in Masciola, *et al.* [24], but a brief overview of the models is given as follows:

- The wave forces were evaluated using Morison's equation at even intervals along the square pontoons and cylindrical columns. This is an acceptable estimation for the wave forces provided the column diameter is much smaller than the wave length [27].
- The uncoupled model treats each tendon as a linear spring.
- A lumped mass cable formulation was used to assemble the coupled TLP model. The forces acting on the cable are due to viscous drag, added mass, internal damping, weight and buoyancy.
- The coupled TLP model was compared and validated against commercial simulation tools to ensure the dynamic models provide an accurate representation of the system response [24]. The validation involved OrcaFlex to model both the platform motion and dynamic mooring line force, and WAMIT to capture the hydrodynamic radiation, diffraction and frequency dependent added mass coefficients.

To proceed with the simulations, a Bretschneider spectrum with a significant wave height of $H_s = 5$ meters and an average period of $T_{avg} = 15$ seconds is used to generate the wave height time histories. The wave direction aligned with the platform surge axis; therefore, the surge, heave and pitch degreesof freedom are excited. In Figures 5 and 6, the platform time history in the surge, heave and pitch directions, as well as the tendon tension, are given for the two TLP test cases at 600 meters and 1200 meters water depth. Accompanying each time history is the corresponding Power Spectral Density (PSD) plot to help identify the frequency range where disagreements show. The TLP properties used in this exercise is based on the data in Table 1.

6.1 Depth = 600 meters

The time histories for a TLP in 600 meters depth is depicted in Figure 5, and in accordance with the results in Table 4, the coupled and uncoupled TLP models agree well. The fairlead tension in one tendon and its corresponding PSD plot for the 600 meter TLP is given in Figure 5a. Although the tendon force condition is violated for the heave and pitch directions, the two TLP systems appear to be nearly identical because the cable natural frequencies are not being excited. This excitation can occur through cable snap loads, interactions with the surface waves, or coupling with the platform natural frequencies. As demonstrated in Figure 3, the gap between the longitudinal cable natural frequencies and the wave band expands as water depth decreases.

The sole difference between the coupled and uncoupled model occurs at the platform pitch natural frequency, as identified by the arrow in Figure 5d. Because Ω_θ is larger than Ω_z, the pitch direction reveals the first symptoms in terms of model difference. The tendon tension also shows a disparity at the pitch natural frequency. The heave natural frequency is less likely to reveal differences because the buoyancy stiffness–to–tendon stiffness ratio Ω_z is smaller than Ω_θ, making the system less sensitive to small variations in tendon tension in that degree of freedom.

6.2 Depth = 1200 meters

In the second case being evaluated, the TLP is in 1200 meter water depth. Six conditions are violated in this scenario: a) the tendon force condition in heave and pitch; b) the frequency condition in surge and yaw; c) and both stiffness conditions. This would lead one to expect the following discrepancies to occur:

- The heave and pitch directions may show difference since Ω_z and Ω_θ have increased.
- The amplitude of surge motion may reduce because cable damping (due to viscous drag) can no longer be ignored.

The disagreements projected in Table 4 can be observed in the platform displacement time history and PSD plots shown in Figures 6b, 6c and 6d, with differences in surge and pitch most apparent. As anticipated by the analytical model, the two models encounter differences in surge direction because the drag force on the cables is significant enough to alter the platform response. This additional damping is created by the fluid cross–flow drag on the cables. The increase in water depth also impacts the mooring lines stiffness. As depth increases, the tendons soften, and this increases the platform sensitivity to disturbances. This impact can be seen in Figure 6c, where the arrow indicates one event in which a series of high frequency fluctuations are present in the coupled model heave response.

In the tension PSD plots, the figures show a series of high frequency amplitudes in the coupled model, the first of which is identified by an arrow. These frequencies are equal to $f_n = n\frac{c_z}{2L}$, where $n = 1, 2, \cdots$, is an integer, and f_n represents the longitudinal cable excitation frequency. Although small in amplitude, these frequencies can contribute significant differences between models, especially if they fall within the wave band frequencies or if a snap load (and the ensuing cable rapid re–tensioning) episode is encountered. As Ω_z or Ω_θ increases, the high frequency cable disturbances are more likely to be observed in heave or pitch directions. These peaks are not present in the uncoupled system, as this model does not have the ability to model cable structural dynamics.

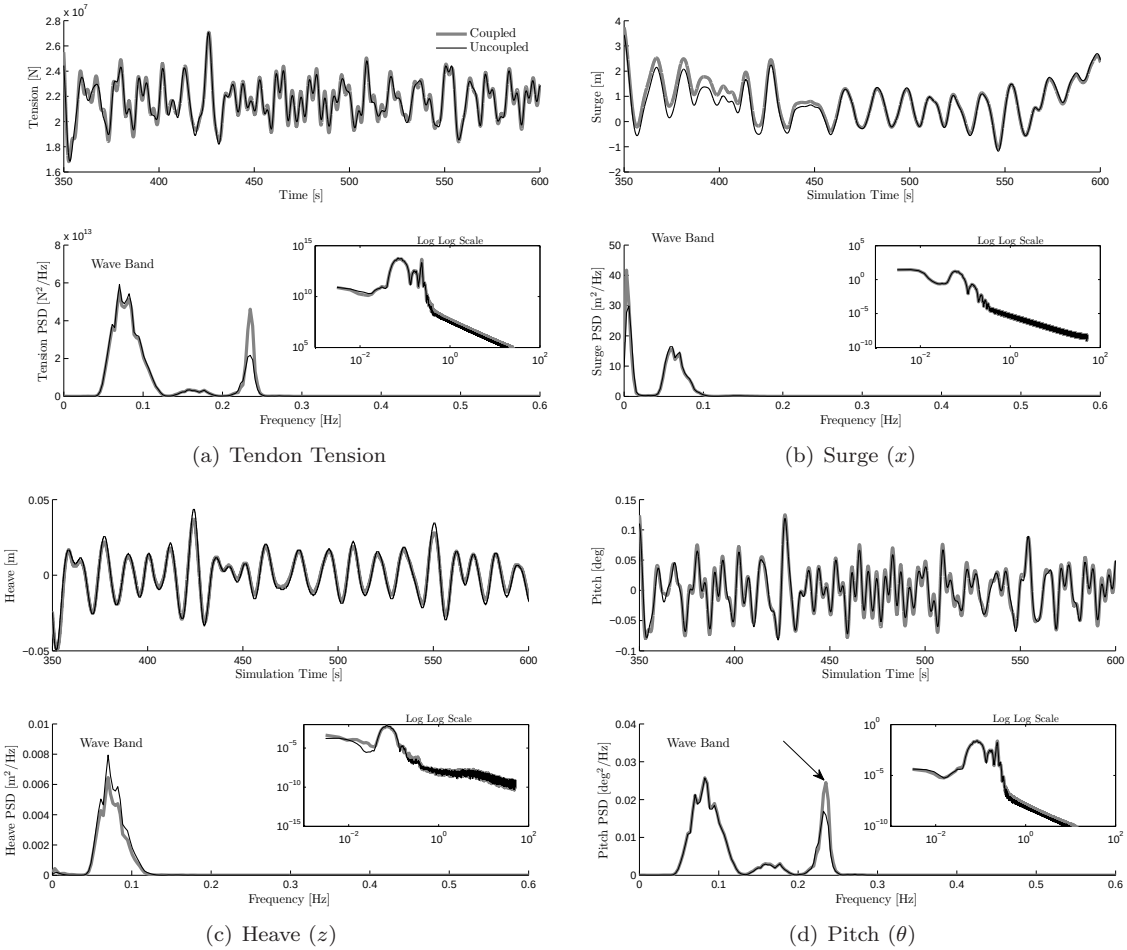

(a) Tendon Tension

(b) Surge (x)

(c) Heave (z)

(d) Pitch (θ)

Figure 5: The above figures illustrate results for weakly coupled TLP in 600 meters water depth. Although differences between the uncoupled and coupled are small when comparing the time histories, the PSD plots help to elucidate the source of model differences. In the pitch PSD plot, a difference between models emerges at the pitch natural frequency since Ω_θ has approached a critical threshold.

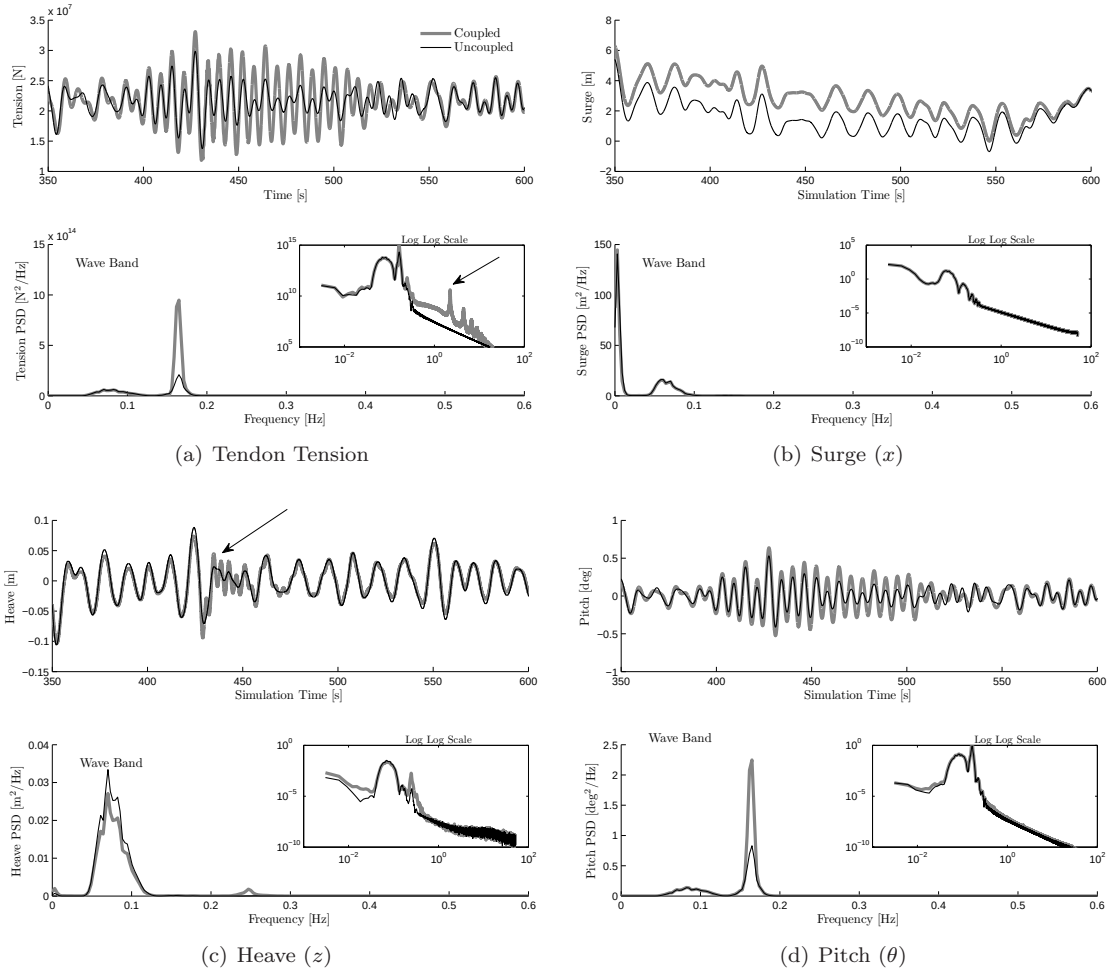

(a) Tendon Tension

(b) Surge (x)

(c) Heave (z)

(d) Pitch (θ)

Figure 6: Simulation results for a TLP in 1200 meters water depth. In this example, the coupled TLP response is more receptive to the cable dynamics. Differences between the coupled and uncoupled models are attributable to 1) the stiffness condition being violated, 2) the platform sensing the mooring drag force, and 3) the cable natural frequencies being excited.

7 Conclusion

This paper outlines the mechanisms promoting similarity between a coupled and an uncoupled TLP model using dimensionless analytical models. These results are intended to be used as a means for highlighting the importance of tendon dynamics in a TLP system and to convey a general awareness of the differences that may occur between coupled and uncoupled TLP numerical models. Alternatively, these results can be used to justify the practice of using massless springs in place of a coupled analysis. We have used one–dimensional wave equations to model the tendon dynamics in the a) longitudinal direction and b) transverse direction. A total of eight conditions must be met to achieve agreement. These conditions, which are presented in Table 4, are: a) tendon force condition; b) frequency condition; c) stiffness condition. The tendon force condition ensures that the dissipative forces are equal to or greater than to the internal forces. If this criterion is not met, the TLP may respond to the high frequency longitudinal waves propagating in the mooring line. The second criteria, the frequency condition, signals that the platform will sense cable damping. If violated, the surge/sway or yaw degrees of freedom will experience damped oscillations. The third condition is in place to measure platform sensitivity to wave height variations. Generally, as tendon stiffness increases relative to the buoyant stiffness, the likelihood of the models agreeing is increased.

In the results derived, the platform mass–to–cable mass ratio appears implicitly through interactions of τ_i^{-1} and $\tilde{\omega}_i^c$. Although the cable and platform mass are helpful in assessing the importance in the tendon and platform coupling, this study shows other parameters, such as cable damping and the relative buoyant/tendon stiffness ratio, also have a role in gauging the importance of the mooring line dynamics. A key element driving the agreement between the coupled and uncoupled models is the buoyancy–to–cable stiffness ratio. As water depth increases, each condition highlighted in Table 4 is more likely to be violated, an observation that is in accordance with earlier findings in Mekah [14].

References

[1] Paulling, J.R., 1971. "*Analysis of the Tension Leg Platform.*" Society of Petroleum Engineers, September, Vol. 1, No. 3, pp. 285-294.

[2] Chandrasekaran, S., and Jain, S.K., 2002, "*Dynamic Behaviour of Square and Triangular Offshore Tension Leg Platform Under Regular Wave Loads.*" Ocean Engineering 29, pp. 279-313.

[3] Musial, W., Butterfield, S., and Boone, A., 2004. "Feasibility of Floating Platform Systems for Wind Turbines." 23^{rd} ASME Wind Energy Symposium, Reno, Nevada, USA.

[4] Low, Y.M., 2009. "*Frequency domain analysis of a tension leg platform with statistical linearization of the tendon restoring force.*" Marine Structures, 22, pp. 480–503.

[5] Jonkman, J.M., 2009. "*Dynamics of Offshore Floating Wind Turbines – Model Development and Verification.*" Wind Energy, Vol. 12, pp. 459492.

[6] Sclavounos, P. D., Lee, S., DiPietro, J., Potenza, G., Caramuscio, P. and De Michele G., 2010. "Floating Offshore Wind Turbines: Tension Leg Platform and Taught Leg Buoy Concepts Supporting 3–5 MW Wind Turbines." European Wind Energy Conference EWEC 2010, Warsaw, Poland, April 20–23.

[7] American Petroleum Institutute, 1997. *Recommended Practices for Planning, Designing, and Constructing Tension Leg Platforms.* Document No. API Recomended Practice 2T, American Petroleum Institute, Washington, D.C., USA.

[8] Angelides, D.C., Chen, C., and Will, S.A., 1982."Dynamic Response of Tension Leg Platform." Proceeding of BOSS 1982, pp 100-120, Cambridge, MA.

[9] Malaeb, D.A., 1982. "*Dynamic Analysis of a Tension Leg Platform.*" Ph.D. Thesis, Texas A&M University, USA.

[10] Jefferys, E.R., and Patel, M.H., 1982. "*On The Dynamics of Taut Mooring Systems.*" Engineering Structures, v 4, n 1, pp 37-43.

[11] Venkataramana, K., 1994. "*Earthquake Response of Tension–Leg-Platforms in Steady Currents.*" Earthquake Engineering and Structural Dynamics, v 23, n 1, pp 63-74.

[12] Catterjee, P.C., Das, P.K., and Faulkner, D., 1997. "*A Hydro–Structural Analysis Program for TLPS.*" Ocean Engineering, v 24, n 4, pp 313-334.

[13] Ran, Z., Kim, M.H., and Zheng, W., 1999. "Coupled Dynamic Analysis of a Moored Spar in Random Waves and Currents (Time Domain versus Frequency Domain Analysis)." 17th International Symposium and Exhibit on Offshore Mechanics and Arctic Engineering, July 5-9, pp 194-200, Lisbon, Portugal.

[14] Mekha B.B., Johnson, C.P., and Roesset, J.M., 1996. "*Implications of Tendon Modeling on Nonlinear Response of TLP.*" Journal of Structural Engineering, Vol. 122, No. 2, pp. 142-149.

[15] Oran, C., 1983. "Overall Dynamic Characteristics of Tension Leg Platfom." 15^{th} Annual Offshore Technology Conference, May 2–5. Houston, TX, pp. 507–513.

[16] Datta, T.K., Jain, A.K., 1988. "*Nonlinear Surge Response of a Tension Leg Platform to Random Wave Forces.*" Journal of Engineering Structures, Vol. 10, pp. 204–210.

[17] Ottaviano, E., and Castelli, G., 2010. "A Study on the Effects of Cable Mass and Elasticity in Cable–Based Parallel Manipulators." ROMANSY 18 Robot Design, Dynamics and Control CISM International Center for Mechanical Sciences, Vol. 524, Ch. 1, pp. 149-156.

[18] Grosenbaugh, M.A., 1995. "*On the Dynamics of Oceanographic Surface Moorings.*" Ocean Engineering, Vol. 23, No. 1, pp. 7-25.

[19] Driscoll, F.R., 1999. "*Dynamics of a Vertically Tethered Marine Platform.*" Ph.D. Thesis, University of Victoria, Canada.

[20] Nordgren, A.P., 1987. "*Analysis of High-Frequency Vibration of Tension Leg Platforms.*" Journal of Offshore mechanics and Artic Engineering, Vol. 109, No. 2, pp. 119-125.

[21] Dong, Y., Xie, G., and Lou, Y.K., 1992. "*Stability of Vortex-Induced Oscillations of Tension Leg Platform Tethers.*" Ocean Engineering. Vol. 19, No. 6, pp. 555-571.

[22] Caughey, T.K., 1963. "*Equivalent Linearization Techniques.*" Journal of the Acoustical Society of America. Vol. 35, No. 11.

[23] French, A.P., 1971. *Vibrations and Waves.* W.W. Norton and Company, New York, NY.

[24] Masciola, M.D., Nahon, M., and Driscoll, F.R., 2011. "*Dynamics Analysis of a Coupled and an Uncoupled Tension Leg Platform.*" Submitted for review to *Marine Structures.*

[25] Farlow, S.J., 1982. *Partial Differential Equations for Scientists and Engineers.* John Wiley and Sons, New York, NY.

[26] Newman, J.N., 1977. *Marine Hydrodynamics.* The Massachusetts Institute of Technology Press, Cambridge, MA.

[27] Chen, X., Ding, Y., Zhang, J., Liagre, P., Niedzwecki, J., and Teigen, P., 2006."*Coupled Dynamic Analysis of a Mini TLP: Comparison with Measurements.*" Ocean Engineering 33, pp. 93117.